Bayesian inversion for source mechanisms of microearthquakes

Hongliang Zhang, and Kristopher A. Innanen

ABSTRACT

We develop a Bayesian approach to simultaneously estimate source mechanisms for a set of microearthquakes, in which uncertainties of model parameters are vigorously quantified. To overcome limitations associated with the use of conventional moment-tensor inversion for low-magnitude events, we use a physically based shear-tensile crack model to characterize the seismic source in the inversion. The shear-tensile model consists of four parameters, strike, dip, rake and slope, to represent a superposition of a shear slip along the fault and a crack opening/closure. In the inversion, normalized displacement amplitudes of direct P-wave are used as observations. The Bayesian inference is employed via Markov-chain Monte Carlo (McMC) sampling with parallel tempering, and the principal component diminishing adaption is also used to ensure efficient sampling. In addition, to reduce the number of modes in 2D posterior marginals and avoid one-side distributed marginals for strike, new prior bounds are applied for strike ($0° - 180°$) and dip ($0° - 180°$). We apply the Bayesian inversion to a passive seismic dataset acquired during a four-well hydraulic-fracture completion program. For three representative events, uncertainties are quantified through posterior distributions of shear-tensile model parameters. The resulting source mechanisms are highly consistent results with a previous study, indicative of the effectiveness of the proposed algorithm.

INTRODUCTION

As a mathematical description for seismic sources, the seismic moment tensor has been extensively used in source studies for various seismic events such as natural tectonic earthquakes, volcanic earthquakes and anthropogenic seismicity. In addition to the classic double couple (DC) that is related to the shear slip along the fault, the moment tensor can also characterize more complex faulting/rupture processes (e.g., tensile faulting and noncoplanar faulting) through the non-DC components (Miller et al., 1998; Wang et al., 2018). While for low-magnitude events (e.g., microearthquakes), the use of conventional moment-tensor inversion may yield unstable results and spurious non-DC components due to the generally low signal-to-noise ratio (Pesicek et al., 2012; Wang et al., 2019), which will further impact the interpretation. For this problem, a physically based shear-tensile crack model was proposed to characterize the seismic source mechanism, in which the source is described by simultaneous in-plane slip and crack opening/closure. Due to less model parameters in comparison with the moment tensor, the use of shear-tensile model can produce more constrained but stable source-mechanism solutions. In addition, the requirement for azimuthal coverage of stations in the source determination process is also reduced with the adoption of shear-tensile model (Šílenỳ et al., 2014; Šílenỳ, 2018; Petružálek et al., 2018).

Most seismic source-mechanism studies use deterministic algorithms to invert for moment tensors, which lacks necessary uncertainty evaluation. To rigorously quantify the uncertainties of source mechanisms, a number of Bayesian inversion approaches have been

developed, for example, Pakzad et al. (2020) employed a Bayesian framework using an McMC algorithm to estimate moment-tensor solutions, in which constraints were applied for first-motion polarities and double couple percentage. Mustać and Tkalčić (2016) implemented a hierarchical Bayesian inversion for moment tensors of moderate-size earthquakes. In addition to moment-tensor parameters, they also treated centroid location and noise as unknown.

In this study, we present a Bayesian inversion approach to simultaneously estimate shear-tensile focal mechanisms of multiple microearthquakes. The Bayesian inversion treats shear-tensile model parameters as well as noise standard deviation as unknown. To avoid one-side distributed posterior marginals for strike and reduce the number of modes presented on 2D posterior marginals, new prior bounds for strike and dip are used. To validate the propose algorithm, we will apply it to a passive seismic dataset acquired during a four-well hydraulic-fracturing completion program in Duvernay Shale.

METHOD

Shear-tensile crack model

We use shear-tensile crack model to characterize source mechanisms of microearthquakes. This model has four independent parameters, strike ($0° - 360°$), dip ($0° - 90°$), rake ($-180°$ $- 180°$) and slope ($-90° - 90°$). The slope represents the angle between the slip direction and the fault plane with values ranging between $-90°$ and $90°$. A value of $0°$ for slope denotes the pure shear source, and values of $-90°$ and $90°$ represent tensile closure and opening, respectively (Vavryčuk, 2001).

In homogenous media, the far-field P-wave displacement caused by a shear-tensile crack can be expressed as (Ou, 2008)

$$\mathbf{u}^P = \frac{\mu A \Delta \dot{u}(t - r/\alpha)}{4\pi\rho\alpha^3} \frac{\hat{\mathbf{r}}^T \mathbf{S} \hat{\mathbf{r}}}{r} \hat{\mathbf{r}}, \tag{1}$$

where μ, A, ρ and α represent shear modulus, rupture area, density and P-wave velocity, respectively; r is the distance between source and receiver; $\hat{\mathbf{r}}$ is a unit vector pointing from source to receiver; $\mathbf{S}$ is the source dislocation tensor; and $\Delta\dot{u}(t)$ is the time derivative of the magnitude of dislocation. The six independent elements of $\mathbf{S}$ are

$$
\begin{aligned}
S_{11} &= [2\sigma/(1-2\sigma) + 2\sin^2\delta\sin^2\phi]\sin\gamma - (\sin\delta\cos\lambda\sin 2\phi + \sin 2\delta\sin\lambda\sin^2\phi)\cos\gamma \\
S_{22} &= [2\sigma/(1-2\sigma) + 2\sin^2\delta\cos^2\phi]\sin\gamma + (\sin\delta\cos\lambda\sin 2\phi - \sin 2\delta\sin\lambda\cos^2\phi)\cos\gamma \\
S_{33} &= [2\sigma/(1-2\sigma) + 2\cos^2\delta]\sin\gamma + \sin 2\delta\sin\lambda\cos\gamma \\
S_{12} &= -\sin^2\delta\sin 2\phi\sin\gamma + (\sin\delta\cos\lambda\cos 2\phi + \sin 2\delta\sin\lambda\sin 2\phi/2)\cos\gamma \\
S_{13} &= \sin 2\delta\sin\phi\sin\gamma - (\cos\delta\cos\lambda\cos\phi + \cos 2\delta\sin\lambda\sin\phi)\cos\gamma \\
S_{23} &= -\sin 2\delta\cos\phi\sin\gamma - (\cos\delta\cos\lambda\sin\phi - \cos 2\delta\sin\lambda\cos\phi)\cos\gamma
\end{aligned}
\tag{2}
$$

where ϕ, δ, λ and γ are the strike, dip, rake and slope, respectively, and σ is the Poisson's ratio, which is fixed and assumed to be 0.25 in the inversion.

Here, the focal mechanism inversion is based on the displacement amplitude of direct P-wave. The observed P-wave amplitudes are scaled over the maximum amplitude. In terms of the modeling data, when the same normalization is applied, the first term in equation (1) for different stations are approximately the same, and thus can be canceled out. In the data pre-processing, an approximate geometrical spreading term $(1/r)$ is applied to the observed data, thus the normalization (i.e., scaling over the maximum) for the modeled data only needs to be applied to the radiation pattern $\hat{\mathbf{r}}^T \mathbf{S} \hat{\mathbf{r}}$. In this study, an isotropic 1-D layered velocity model is used for ray tracing in order to estimate the take-off angles. The vector $\hat{\mathbf{r}}$ is calculated based on the azimuth measured from source to receiver and the take-off angle at the source.

Bayesian inversion

In this study, we carry out Bayesian inversion to simultaneously estimate the shear-tensile focal mechanisms for a set of microearthquakes. Based on Bayes' theorem, the posterior probability density (PPD) is defined as

$$P(\mathbf{m}|\mathbf{d}) \propto P(\mathbf{m})P(\mathbf{d}|\mathbf{m}), \tag{3}$$

where $\mathbf{m}$ represents the model vector. For M microearthquakes, $\mathbf{m}$ is $[\phi_1, \delta_1, \lambda_1, \gamma_1, \phi_2, \delta_2, \lambda_2, \gamma_2, \ldots, \phi_M, \delta_M, \lambda_M, \gamma_M]$. $P(\mathbf{m})$ denotes the priori probability. $P(\mathbf{d}|\mathbf{m})$ is interpreted as the likelihood function, $L(\mathbf{m})$, when $\mathbf{d}$ represents the observed data. In this research, $\mathbf{d}$ is the data vector consisting of the measured normalized P-wave amplitudes. Under the assumptions of Gaussian-distributed errors and the negligible off-diagonal terms of the data covariance matrix, the likelihood function can be expressed as

$$L(\mathbf{m}) = \prod_{k=1}^{M} \frac{1}{(2\pi)^{N_k/2} \sigma_k^{N_k}} \exp\left[-(\mathbf{d}_k - g(\mathbf{m}_k))^T (\mathbf{d}_k - g(\mathbf{m}_k))/(2\sigma_k^2)\right], \tag{4}$$

where σ_k is the standard deviation of noise for the kth event, and N_k is the number of observed data for this event. g is the forward model in the isotropic, layered medium. In the Bayesian inversion, the noise standard deviation for each event is unknown and is also estimated by the McMC sampling.

In the Bayesian inversion, the Metropolis-Hasting criterion is used accept or reject the perturbed models based on the PPD. To ensure efficient sampling, the McMC sampling is implemented with parallel tempering and diminishing adaption of a principal axes proposal density (Dosso et al., 2014). In the inversion, the prior is assumed to be uniform for all parameters including noise standard deviations. The shear-tensile model parameters, strike, dip, rake and slope, are conventionally defined within the ranges of $0° - 360°$, $0° - 90°$, $-180° - 180°$ and $-90° - 90°$, respectively. Due to the intrinsic fault-plane ambiguity of the

source-mechanism solution, multiple modes are expected to be observed from the posterior marginal distributions of model parameters, especially for strike-slip mechanisms. In addition, the posterior marginal of the dip angle for vertical or nearly vertical fault plane is only distributed on one side due to the constraint of upper bound (90°) for dip. To reduce the number of modes of posterior marginals and overcome the one-side distribution problem, we modify the prior bounds for strike and dip in this study. Considering that (ϕ_1, δ_1, λ_1, γ_1) and ($\phi_1 \pm 180°$, $180° - \delta_1$, $-\lambda_1$, γ_1) represent the same nodal-plane solution, the prior bounds for both strike and dip can be changed to $0° - 180°$. The problem of one-side marginal for dip will be eliminated due to the increased prior range for dip, and the number of modes will also be reduced due to the narrower prior range for strike.

APPLICATION TO THE FIELD DATA

Datasets

We apply the proposed Bayesian inversion to a passive seismic dataset in the Tony Creek Dual Microseismic Experiment (ToC2ME) (Eaton et al., 2018), in which a diverse set of sensors were used to monitoring multi-stage hydraulic-fracturing operations at a four-well pad west of Fox Creek, Alberta. The recording system consists of 68 shallow-borehole array stations, one strong-motion accelerometer and six broadband seismometers. Hypocenters were well determined for over 4,000 events with moment magnitudes ranging between M_W -1 and M_W 3.2 (Eaton et al., 2018), and moment-tensor solutions for a subset of 530 high-quality events with magnitudes ranging from Mw 1 to Mw 3.2 were estimated (Zhang et al., 2019). Here, we focus on the 530 events for the source-mechanism determination with the proposed algorithm, and only the data acquired with shallow borehole array stations are used. Figure 1 shows the distribution of the 530 events. As marked by different symbols, these events were classified into four groups based on the moment-tensor solutions (Zhang et al., 2019). Two groups of events (marked by circles and diamonds) were characterized by strike-slip mechanisms along either N-S/E-W or NE-SW/NW-SE trending nodal planes. One group of events were found to have NW–SE/NE–SW trending nodal planes exhibiting either oblique dip-slip on subvertical planes or slip on a shallow-dipping plane. The remaining group has a diverse set of source mechanisms that do not fit into any of the previous three major groups.

Results

Using the proposed Bayesian approach, the shear-tensile focal mechanisms for the 530 events are estimated. Here, a representative event (event II in Figure 1) is used to illustrate the effectiveness of the new prior bounds for strike and dip. Figures 2 and 3 show the posterior marginals of the four model parameters before and after the adoption of new prior bounds. In Figure 2, it can be seen that four major modes can be observed from the marginal distribution for strike, that are associated with the two nodal planes. In addition, the dip marginal distribution is only presented on one side due to the upper prior bound. Nevertheless, posterior marginals of all model parameters exhibit Gaussian-like distributions. As can be seen in Figure 3, after applying the new prior bounds the number of modes for strike is reduced, and two-sided Gaussian distribution is presented for dip. These improvements are more evidently seen from scatter plots between strike and the other three
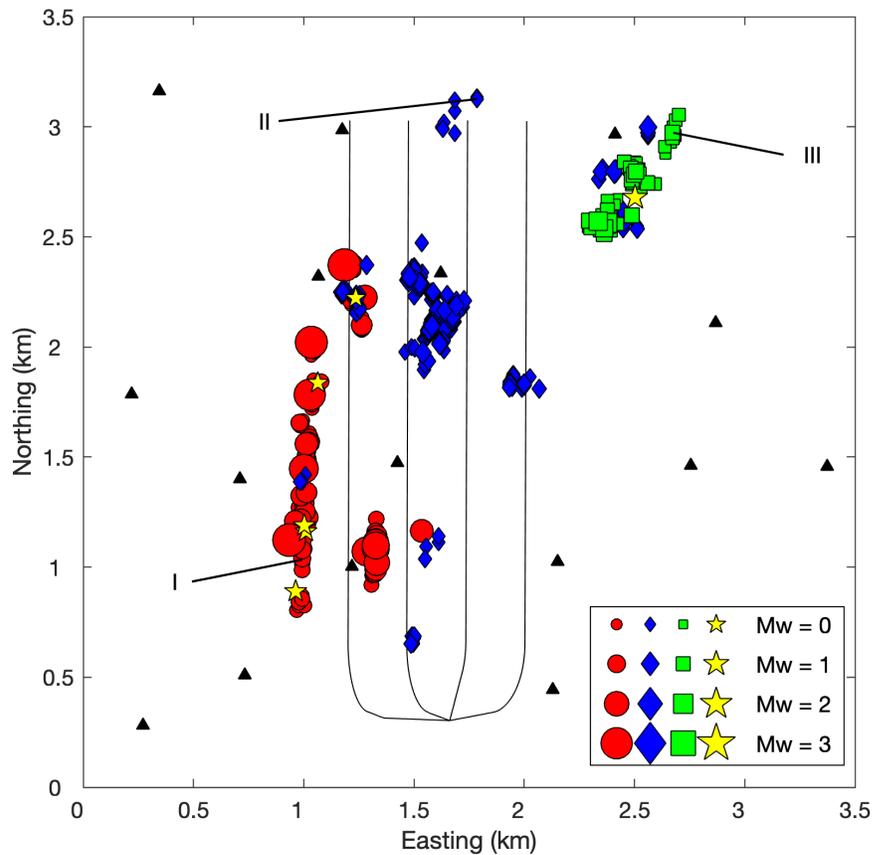
FIG. 1. Distributions of the 530 events used for this study. The four groups of events were marked by different symbols, and triangles represent the shallow borehole-array stations. Three representative events from the first three groups that will be further analyzed in this study are marked out. Event symbols are scaled based on the moment magnitude.

model parameters (Figures 4 and 5). Based on the two distinct clusters in the scatter plots in Figure 5, two nodal-plane solutions can be easily separated by a simple screening for strike. Then further uncertainty analysis can be implemented based on the posterior marginals for either of the two nodal planes. Figure 6 shows the model-parameter marginals for nodal plane 1 (red cluster in Figure 5).

Next, we select three representative events from the three major groups for further uncertainty analysis. Figures 7 –9 show the scatter plots as well as posterior marginals for the three events. For all the three events, two clear nodal-plane solutions can be identified from these three figures. For event III, widely distributed outliers marked by green color can also be seen from the scatter plots (Figures 9 (a-c)), while the posterior marginals for outliers are negligible compared with the two nodal planes. For each of the three representative events, we select only one the nodal plane for uncertainty analysis based on the posterior marginals. Table 1 shows the 95% credibility intervals for strike, dip, rake and slope. For the sake of comparison, the nodal plane solutions obtained through a full moment-tensor inversion by Zhang et al. (2019) are also presented in Table 1. It can be observed that the
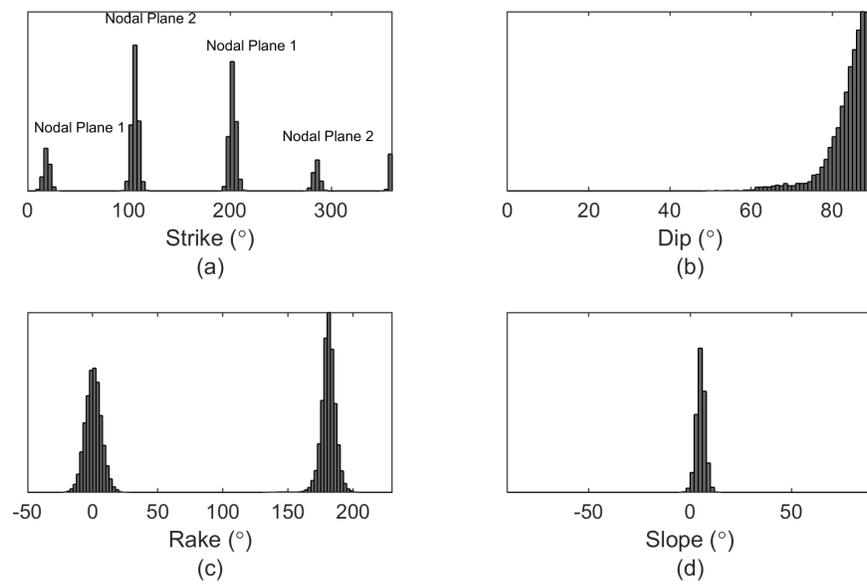
FIG. 2. Marginal distributions for (a) strike, (b) dip, (c) rake and (d) slope of one representative event before using the new prior bounds for strike and dip.
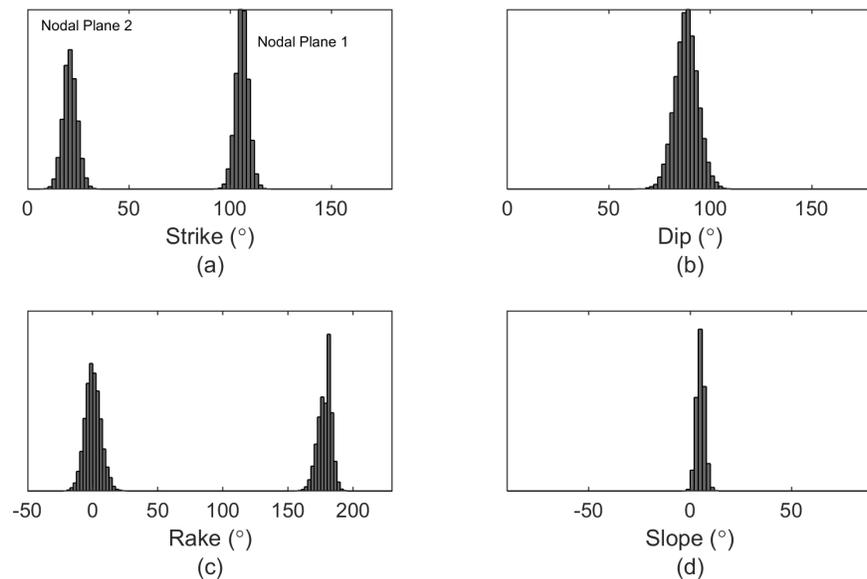
FIG. 3. Marginal distributions for (a) strike, (b) dip, (c) rake and (d) slope of one representative event after using the new prior bounds for strike and dip.

proposed Bayesian inversion yields highly consistent nodal-plane solutions with the previous study. In addition, the source mechanism with uncertainty can also be represented by the so-called fuzzy beachball, in which uncertainty regions of nodal planes are indicated by blurred areas. Figures 10 and 11 show the fuzzy double-couple solutions and moment tensors for the three representative events, in which solutions with mode values are represented by black lines.
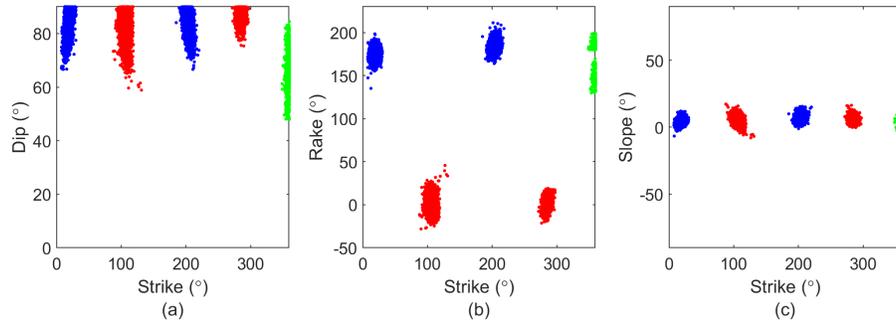
FIG. 4. Scatter plots between (a) strike and dip, (b) strike and rake and (c) strike and slope. Red and blue dots are associated with nodal plane 1 and nodal plane 2, respectively. Green dots denote outliers. These results are obtained before applying new prior bounds for strike and dip.
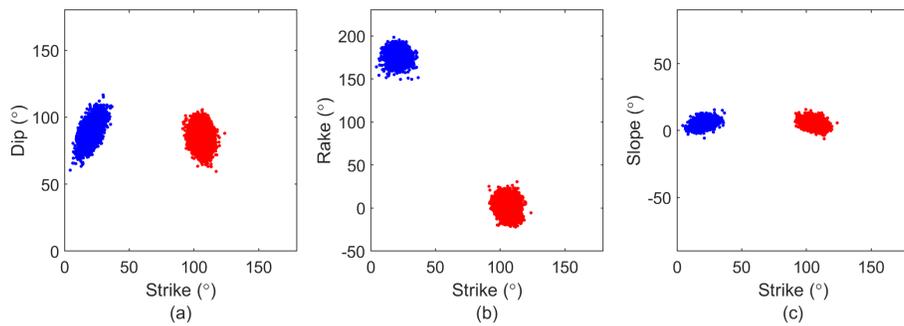
FIG. 5. Scatter plots between (a) strike and dip, (b) strike and rake and (c) strike and slope. Red and blue dots are associated with nodal plane 1 and nodal plane 2, respectively. These results are obtained after applying new prior bounds for strike and dip.
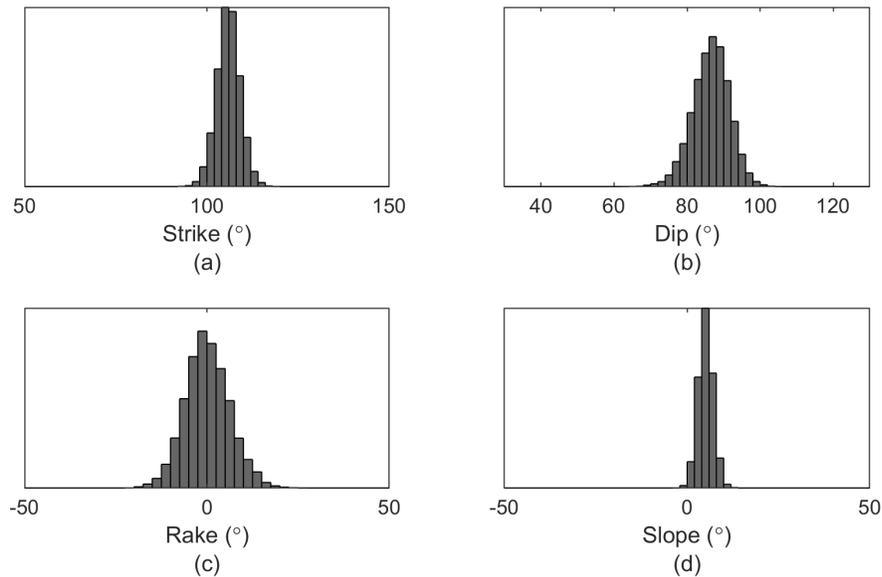
FIG. 6. Posterior marginal distributions of (a) strike, (b) dip, (c) rake and (d) slope for nodal plane 1 (red cluster in Figure 5).
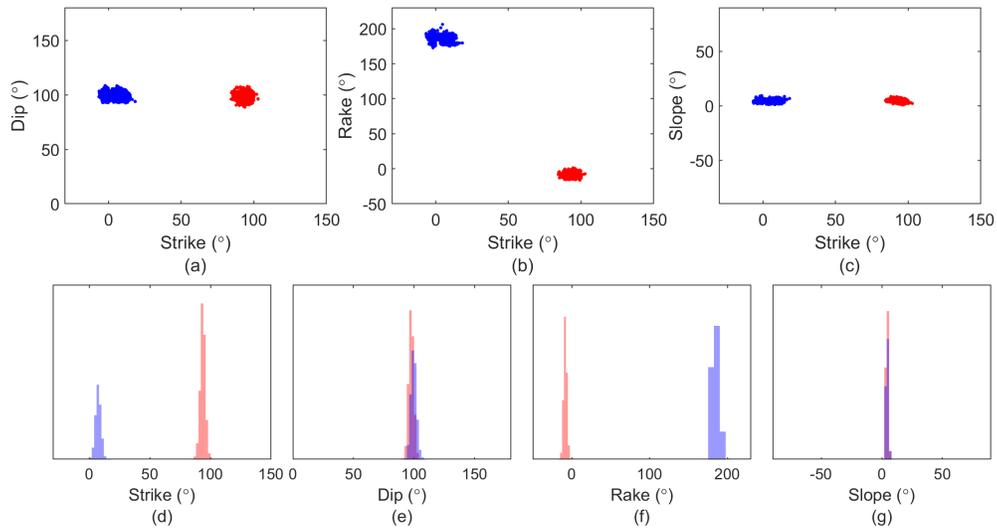
FIG. 7. Inversion results for event I in Figure 1. (a-c) Scatter plots between strike and the other three model parameters. (d-g) Posterior marginals of model parameters for shear-tensile source mechanism. Red and blue colors represent the results associated with two nodal planes.
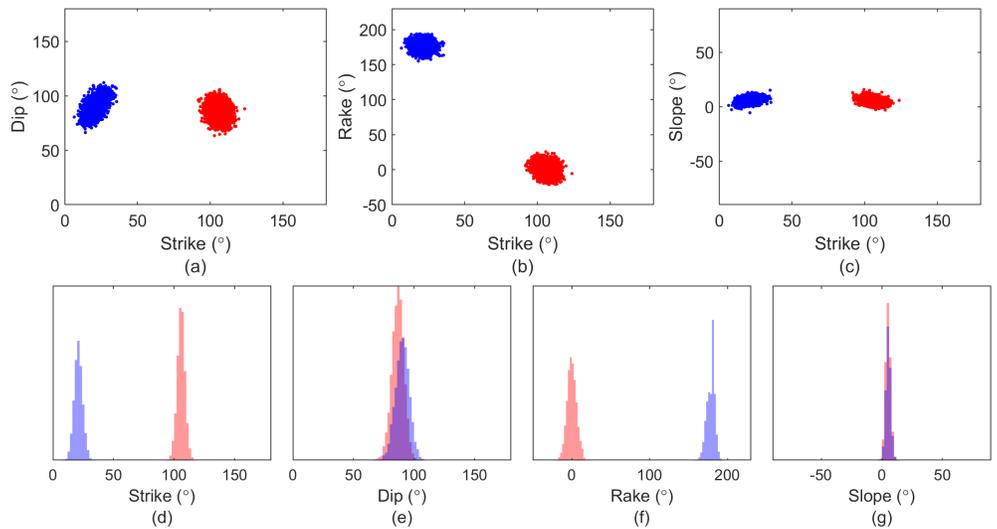
FIG. 8. Inversion results for event II in Figure 2. (a-c) Scatter plots between strike and the other three model parameters. (d-g) Posterior marginals of model parameters for shear-tensile source mechanism. Red and blue colors represent the results associated with two nodal planes.

Table 1. 95% credibility intervals of nodal plane solutions obtained in this study and solutions from Zhang et al. (2019).

Event No.	Strike (°)	Dip (°)	Rake (°)	Slope (°)	Strike (°)	Dip (°)	Rake (°)	Slope (°)
I	[89.3, 97.5]	[93.5, 101.8]	[-12.4, -4.2]	[2.7, 6.1]	94.1	96.4	-5.8	4.3
II	[99.4, 112.2]	[76.1, 95.9]	[-11.4, 12.8]	[1.2, 9.1]	109.5	86.9	0.0	-7.9
III	[99.1, 112.6]	[92.1, 102.3]	[-55.4, -40.5]	[9.2, 12.7]	108.7	93.3	-43.7	12.6
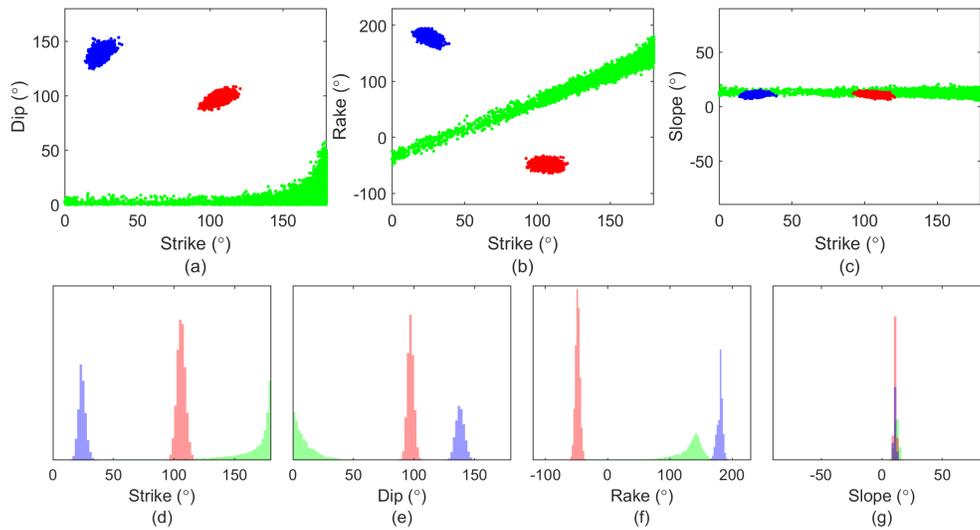
FIG. 9. Inversion results for event III in Figure 1). (a-c) Scatter plots between strike and the other three model parameters. (d-g) Posterior marginals of model parameters for shear-tensile source mechanism. Red and blue colors represent the results associated with two nodal planes, and green color represents outliers.
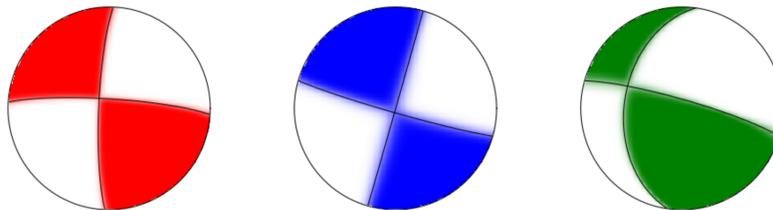
FIG. 10. Fuzzy beachball diagrams for the double-couple components of the three representative events.
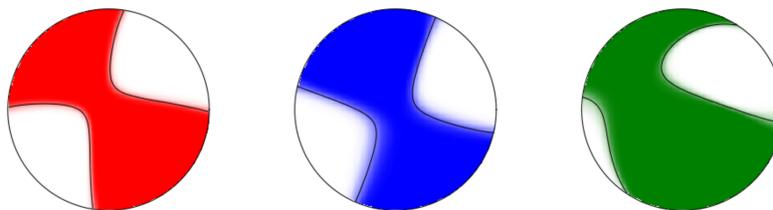
FIG. 11. Fuzzy beachball diagrams for the moment-tensor solutions of the three representative events.).

CONCLUSIONS

We have presented a probabilistic approach to simultaneously estimate shear-tensile source mechanisms for multiple microearthquakes. The Bayesian inference has been employed via McMC sampling with parallel tempering and the principal component diminishing adaption to ensure efficiency sampling. Compared with conventional full moment-tensor inversion for low-magnitude events, the use of shear-tensile crack model tends can yield more robust results due to less model parameters. In addition, the use of conventionally defined ranges for strike and dip may generate one-side distributed marginals for strike and multiple modes from 2D marginals. To overcome these limitations, new prior bounds for strike ($0° - 180°$) and dip ($0° - 180°$) have been used in the Bayesian inversion. The effectiveness of the proposed method has been demonstrated through the application the ToC2ME dataset, in which three representative events are used for detailed analysis. In the future research, we will analyze the inversion results for all the 530 high-quality events within ToC2ME dataset.

ACKNOWLEDGEMENTS

REFERENCES

Dosso, S. E., Dettmer, J., Steininger, G., and Holland, C. W., 2014, Efficient trans-dimensional bayesian inversion for geoacoustic profile estimation: Inverse Problems, **30**, No. 11, 114,018.

Eaton, D. W., Igonin, N., Poulin, A., Weir, R., Zhang, H., Pellegrino, S., and Rodriguez, G., 2018, Induced seismicity characterization during hydraulic-fracture monitoring with a shallow-wellbore geophone array and broadband sensors: Seismological Research Letters, **89**, No. 5, 1641–1651.

Miller, A. D., Foulger, G., and Julian, B. R., 1998, Non-double-couple earthquakes 2. observations: Reviews of Geophysics, **36**, No. 4, 551–568.

Mustać, M., and Tkalčić, H., 2016, Point source moment tensor inversion through a bayesian hierarchical model: Geophysical Journal International, **204**, No. 1, 311–323.

Ou, G.-B., 2008, Seismological studies for tensile faults: TAO: Terrestrial, Atmospheric and Oceanic Sciences, **19**, No. 5, 4.

Pakzad, M., Khalili, M., and Vahidravesh, S., 2020, An mcmc bayesian full moment tensor inversion constrained by first-motion polarities and double couple percent: Solid Earth Discussions, 1–27.

Pesicek, J., Sileny, J., Prejean, S., and Thurber, C., 2012, Determination and uncertainty of moment tensors for microearthquakes at okmok volcano, alaska: Geophysical Journal International, **190**, No. 3, 1689–1709.

Petružálek, M., Jechumtálová, Z., Kolář, P., Adamová, P., Svitek, T., Šílenỳ, J., and Lokajíček, T., 2018, Acoustic emission in a laboratory: mechanism of microearthquakes using alternative source models: Journal of Geophysical Research: Solid Earth, **123**, No. 6, 4965–4982.

Šílenỳ, J., 2018, Constrained moment tensors: source models and case studies, *in* Moment Tensor Solutions, Springer, 213–231.

Šílený, J., Jechumtálová, Z., and Dorbath, C., 2014, Small scale earthquake mechanisms induced by fluid injection at the enhanced geothermal system reservoir soultz (alsace) in 2003 using alternative source models: Pure and Applied Geophysics, **171**, No. 10, 2783–2804.

Vavryčuk, V., 2001, Inversion for parameters of tensile earthquakes: Journal of Geophysical Research: Solid Earth, **106**, No. B8, 16,339–16,355.

Wang, F., Ma, J., Han, G., Dong, L., and Sun, D., 2019, Investigating factors influencing moment tensor inversion of induced seismicity in virtual iot: IEEE Access, **7**, 34,238–34,251.

Wang, R., Gu, Y. J., Schultz, R., and Chen, Y., 2018, Faults and non-double-couple components for induced earthquakes: Geophysical Research Letters, **45**, No. 17, 8966–8975.

Zhang, H., Eaton, D. W., Rodriguez, G., and Jia, S. Q., 2019, Source-mechanism analysis and stress inversion for hydraulic-fracturing-induced event sequences near fox creek, albertasource-mechanism analysis and stress inversion: Bulletin of the Seismological Society of America, **109**, No. 2, 636–651.